Polymer 72 (2015) 69–81

Contents lists available at ScienceDirect

Polymer

journal homepage: www.elsevier.com/locate/polymer

Conductive films based on composite polymers containing ionic liquids absorbed on crosslinked polymeric ionic-like liquids (SILLPs)

B. Altava [a], V. Compañ [b, *], A. Andrio [c], L.F. del Castillo [d], S. Mollá [b], M.I. Burguete [a], E. García-Verdugo [a], S.V. Luis [a, **]

[a] Universidad Jaume I, Departamento de Química Inorgánica y Orgánica, Av. de Vicent Sos Baynat, s/n, Castellón de la Plana, 12071, Spain
[b] Departamento de Termodinámica Aplicada, Univ. Politécnica de Valencia, Valencia, 46022, Spain
[c] Universidad Jaume I, Departamento de Física., Av. de Vicent Sos Baynat, s/n, Castellón de la Plana, 12071, Spain
[d] Departamento de Polímeros, Instituto de Investigaciones en Materiales, Universidad Nacional Autónoma de México, Ciudad Universitaria, Apartado Postal 70-360, Coyoacán, México, DF, 04510, Mexico

ARTICLE INFO

Article history:
Received 31 March 2015
Received in revised form
2 July 2015
Accepted 6 July 2015
Available online 10 July 2015

Keywords:
Supported ionic liquids
Ionic liquids
Ionic conductivity
Imidazolium
Polymer electrolytes

ABSTRACT

Polymerization of styrenic monomers containing imidazolium subunits in the presence of crosslinking monomers and using ionic liquids (ILs) as porogenic agents provides composite materials with excellent mechanical properties and displaying conductivities that are in the same order of magnitude than those shown by bulk ILs. This approach allows the use of high crosslinking degrees and low IL-loadings without compromising the required properties of the resulting composites. Besides, no appreciable leaching of the bulk IL component is detected.

1. Introduction

The substitution of aqueous electrolytes by electrolytes based on ionic liquids (ILs) to obtain efficient polymer composite membranes has attracted significant interest in the last years [1]. This is due to the unique physical properties of ILs and their high ionic conductivity. Two main strategies have been explored for the preparation of polymeric composite membranes based on ILs. The first one involves the addition of an IL-phase into a polymeric matrix [2]. These membranes are generally prepared by direct polymerization of a structural monomer and/or a crosslinking monomer in the presence of a room temperature IL (RTIL) or, alternatively by coating the corresponding polymeric membrane with the appropriate RTIL. In general, these procedures resulted in materials with good conductivities (ca. 10^{-2} S cm^{-1} at room temperature) depending on the loading and nature of the IL and on polymer composition [3]. However, this approach presents some limitations due to the possible leakage of the IL-electrolyte from the polymeric matrix. A second approach involves the use of the so-called polymerized ionic liquids (PILs) that can be obtained from monomers having ionic liquid-like structures [4]. They can be copolymerized with non-ionic comonomers leading to linear soluble PILs and/or with crosslinking monomeric agents leading to insoluble PILs [5]. Both, soluble and cross-linked poly(ionic liquid) materials have demonstrated to have interesting conductivity properties [6]. Indeed, their properties are highly dependent of the composition and type of the co-monomers used, as well as on the polymer morphology and the nature and length of the spacer linking the backbone and the ionic-liquid-like units [7]. Supported ionic liquid-like phases (SILLPs) have also been obtained by covalently binding IL-like moieties, such as alkylimidazolium cations, to either macroporous or gel-type polystyrene-divinylbenzene resins [8,9]. Partly related imidazolium resins based on polystyrene backbones have been used for different applications like gas separations [10–12]. However, their ionic conductivity drops significantly to values below 10^{-6} S cm^{-1} due to the decrease in the number of the mobile ions. An interesting alternative resides in the merging of both approaches [13,14]. Thus, a monomer bearing an ionic liquid-like fragment can be

* Corresponding author.
** Corresponding author.
E-mail addresses: vicommo@ter.upv.es (V. Compañ), luiss@uji.es (S.V. Luis).

http://dx.doi.org/10.1016/j.polymer.2015.07.009
0032-3861/

polymerized in the presence of an appropriate crosslinking agent and a RTIL. This provides a polymeric backbone containing IL-like moieties to which the IL molecules will be strongly associated. This approach can allow combining the advantages found for the two former alternatives and eliminating, or at least minimizing, the potential leaching of the bulk IL phase. Besides, the resulting properties of these composites, in particular their conductivity, can be tailored by the proper selection of the polymeric and liquid components, in particular by a selection of the elements defining the interaction between the different IL-based subunits (anions and cations). In this context, the use of ILs as porogenic agents has been demonstrated to be very useful for the preparation of monolithic macroporous polymers with tailored porous structures [15] and the polymerization of a combination of polymerizable divynilic ionic liquids with cellulose dissolved in an IL with has been investigated for the generation of new kinds of promising ion-gel-type composite materials [16].

Here we present our results on the synthesis and characterization of different crosslinked polymeric films bearing ionic liquid-like units in the polymeric network and obtained in the absence and presence of additional absorbed ILs. Films with different IL/polymer ratios have been investigated, with the aim of understanding the influence of the interactions between the liquid and the solid ionic phase on the functional properties of the composites.

2. Experimental

2.1. Materials

All reagents were used as purchased from commercial suppliers without further purification. The liquid monomer **1** (VBIM [NTf_2], 1-(4-vinylbenzyl)-3-butyl imidazolium bistriflamide) was synthesized following the procedure previously described [17]. Commercially available 1-butyl-3-methylimidazolium chloride ([BMIM][Cl] (**2a**) was purchased from Merck, while [1-butyl-3-methylimidazolium bis(trifluoromethylsulfonyl)imide] [BMIM][NTf_2] (**2b**) was prepared by the exchange of chloride by NTf_2^- using $LiNTf_2$, according to the general experimental methodology described in the literature [18]. FTIR spectra were acquired with a MIRacle single-reflection ATR diamond/ZnSe accessory in a Jasco FT-IR 6200. Raman spectra were acquired on a JASCO NRS-3100 dispersive spectrometer under the following conditions: 785 nm laser with a single monochromator, grating 600 lines·mm^{-1}, slit 0.2 mm, resolution 12.75 cm^{-1}, with a centre wavenumber of 1200 cm^{-1}, a laser power of 90.1 mW, and ten accumulations of 5 s each. Elemental analyses were performed on a LecoTuSpect Micro instrument. Differential scanning calorimetry (DSC) analyses were obtained using a Mettler-Toledo 831-DSC device at 10 K/min, under a nitrogen atmosphere in the −70 to 80 °C range for the different films. For all DSC measurements, at least three heating and cooling cycles were carried out and data were obtained from the third cycle.

2.2. General procedure for the synthesis of the films *F1*–*F3*

A mixture of VBIM [NTf_2] **1**, trimethylolpropane trimethacrylate **3** and 1 wt% of AIBN (as the initiator) was stirred and ultrasonicated to obtain a homogeneous solution that was then cast into a glass mold. The solution containing monomers, cross-linkers, AIBN and IL was introduced in the narrow space created between two microscopy slides separated by two thin lamellas (see Fig. 1). Polymerization was then carried out for 24 h at 65 °C in an oven. Afterwards, the films were removed mechanically from the molds and thoroughly washed with organic solvents. The resulting polymers were homogeneous, transparent and ca. 4–5 cm × 1.5–2 cm in size, with a thickness of about 130 ± 10 μm. Nitrogen elemental analysis was used to obtain the final IL-loading of the polymers. In all cases, the experimental nitrogen percentage obtained was in good agreement with the expected values.

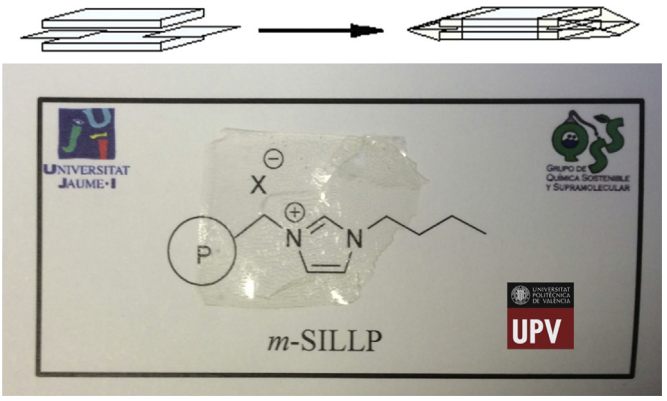

Fig. 1. Procedure for the preparation of polymeric films. Appearance of a representative film.

F1: 60 wt% of VBIM [NTf_2] **1** and 40 wt% of trimethylolpropane trimethacrylate **3**. FT-IR (ν cm^{-1}): 3146, 3119, 2965, 2887, 1719, 1464, 1350, 1328, 1182, 1132, 1055, 614. RAMAN (ν cm^{-1}): 1637, 1613, 1449, 1420, 1351, 1330, 1267, 1242, 1208, 1188, 1136, 1117, 1056, 1027, 830, 744, 644, 616, 595, 574. IL-loading calculated by elemental analysis: 1.1 mmol IL/g of polymer (1.1 theoretical) (ca. 1 mmol of ions/mL) (Elemental analysis for N: experimental 5.2; calculated: 4.9%).

F2: 70 wt% of VBIM [NTf_2] **1** and 30 wt% of trimethylolpropane trimethacrylate **3**. FT-IR (ν cm^{-1}): 3152, 3115, 2966, 2937, 2879, 1725, 1564, 1346, 1321, 1182, 1131, 1051, 614. RAMAN (ν cm^{-1}): 1630, 1613, 1450, 1421, 1354, 1329, 1268, 1242, 1207, 1188, 1136, 1118, 1056, 1027, 831, 743, 643, 614, 593, 574. IL-loading calculated by elemental analysis: 1.3 mmol IL/g of polymer (1.3 theoretical) (ca. 1.1 mmol of ions/mL) (Elemental analysis for N: experimental 5.7; calculated: 5.7%).

F3: 77 wt% of VBIM [NTf_2] **1** and 23 wt% of trimethylolpropane trimethacrylate **3**. FT-IR (ν cm^{-1}): 3152, 3107, 2966, 2938, 2882, 1725, 1564, 1346, 1321, 1182, 1131, 1051, 614. RAMAN (ν cm^{-1}): 1630, 1611, 1449, 1419, 1353, 1328, 1266, 1241, 1207, 1187, 1135, 1117, 1056, 1025, 832, 742, 642, 614, 593, 573. IL-loading calculated by elemental analysis: 1.6 mmol IL/g of polymer (1.7 theoretical) (ca. 1.4 mmol of ions/mL) (Elemental analysis for N: experimental 6.7; calculated: 7.0%).

2.3. General procedure for the synthesis of films *F4*–*F6*

A mixture of VBIM [NTf_2] **1**, trimethylolpropane trimethacrylate **3**, BMIM [NTf_2] **2a** (**F4** and **F5**) or BMIM [Cl] **2b** (**F6**) and 1 wt% of AIBN (as the initiator) was stirred and ultrasonicated to obtain a homogeneous solution which was then cast into a glass mold. Polymerization was then carried out for 24 h at 65 °C in an oven. The films were separated from the glass plates and thoroughly washed with organic solvents and dried before use.

F4: 69 wt% of VBIM [NTf_2] **1**, 11 wt% of trimethylolpropane trimethacrylate **3** and 20 wt% of BMIM [NTf_2] **2a**. FT-IR (ν cm^{-1}): 3153, 3147, 3107, 2965, 2938, 2877, 1725, 1564, 1346, 1321, 1182, 1131, 1051, 614. RAMAN (ν cm^{-1}): 1613, 1565, 1449, 1419, 1386, 1333, 1269, 1242, 1210, 1189, 1136, 1117, 1057, 1026, 830, 744, 643, 625, 575. IL-loading calculated by elemental analysis: 1.8 mmol IL/g of polymer (1.8 theoretical: 1.3 corresponding to the covalently supported imidazolium cations and 0.5 to the presence of **2a**) (ca. 1.5 mmol of ions/mL) (Elemental analysis for N: experimental 7.5; calculated: 7.6%).

F5: 58 wt% of VBIM [NTf_2] **1**, 8 wt% of trimethylolpropane trimethacrylate **3** and 34 wt% of BMIM [NTf_2] **2a**. FT-IR (cm^{-1}): 3151, 3109, 3092, 2965, 2936, 2876, 1726, 1563, 1462, 1349, 1331, 1184, 1135, 1053, 738, 613. RAMAN (ν cm^{-1}): 1613, 1565, 1449, 1419, 1388, 1337, 1242, 1210, 1189, 1136, 1119, 1057, 1026, 830, 744, 645, 627, 606, 575. BMIM [NTf_2] IL-loading calculated by elemental analysis: 1.8 mmol IL/g of polymer (1.9 theoretical: 1.1 corresponding to the covalently supported imidazolium cations and 0.8 to the presence of **2a**) (ca. 1.5 mmol of ions/mL) (Elemental analysis for N: experimental 7.6; calculated: 8.1%).

F6: 59 wt% of VBIM [NTf_2] **1**, 8 wt% of trimethylolpropane trimethacrylate **3** and 33 wt% of BMIM [Cl] **2b**. FT-IR (cm^{-1}): 3151, 3109, 3092, 2965, 2936, 2876, 1726, 1563, 1462, 1349, 1331, 1184, 1135, 1053, 738, 613. RAMAN (ν cm^{-1}): 1613, 1565, 1449, 1419, 1388, 1337, 1242, 1210, 1189, 1136, 1119, 1057, 1026, 830, 744, 645, 627, 606, 575. IL-loading calculated by elemental analysis: 2.9 mmol IL/g of polymer (3.0 theoretical: 1.1 corresponding to the covalently supported imidazolium cations and 1.9 to the presence of **2a**) (ca. 2.5 mmol of ions/mL) (Elemental analysis for N: experimental 9.3; calculated: 10.0%; Elemental analysis for S: experimental 6.7; calculated: 7.2%).

2.4. Impedance measurements

Impedance measurements were carried out on the polymeric films at several temperatures lying in the range 273 K (0 °C)–403 K (130 °C) and within the frequency window $10^{-1} < f < 10^{7}$ Hz. The experiments were performed with 100 mV amplitude, using a Novocontrol broadband dielectric spectrometer (Hundsangen, Germany) integrated by a SR 830 lock-in amplifier with an Alpha dielectric interface. The sample of interest was sandwiched between two gold circular electrodes coupled to the impedance spectrometer acting as blocking electrodes. The assembly membrane-electrode was annealed in the Novocontrol setup under an inert dry nitrogen atmosphere previously to the start of the actual measurement. For this, firstly a temperature cycle from 0 °C to 130 °C to 0 °C, in steps of 10 °C, was carried out. After this, in a new cycle of temperature scan, the dielectric spectra were collected in each step. This was performed to ensure the measurements reproducibility and to eliminate the potential interference of water retained by the composite membranes, in particular taking into account the hygroscopicity of some ILs. During the conductivity measurements, the temperature was maintained (isothermal experiments) or changed stepwise from 0 to 130 °C controlled by a nitrogen jet (QUATRO from Novocontrol) with a temperature error of 0.1 K during every single sweep in frequency.

3. Results and discussion

3.1. Synthesis of poly(ionic) polymeric films

Polymerization of the styrenic monomer containing imidazolium fragments **1** was performed in the presence of trimethylolpropane trimethacrylate (TMPTMA, **3**) as comonomer and crosslinking agent to obtain the corresponding poly(ionic) polymeric films **F1**–**F3**. The corresponding polymeric matrices differed on the degree of crosslinking associated to the content of **3** in the monomeric mixture (from 40 to 13% in weight). Films **F4** and **F5** were obtained in the presence an additional IL-phase. ([BMIM][NTf_2], **2a**) (Scheme 1). In this case, the crosslinking degree ranged from 11 to 8% in weight (ca. 14-12% regarding the ratio monomer:crosslinker) and the amount of BMIM was adjusted to 20 and 34% of the total weight (see Table 1). Finally, **F6** was prepared analogously to **F5** but substituting [BMIM][NTf_2] (**2a**) by [BMIM][Cl] (**2b**).

All prepared polymers were fully characterized by a full set of spectroscopic tools as well as by elemental analysis and differential scanning calorimetry (DCS). Polymers **F1**–**F3** gave excellent elemental analyses, with the values for all elements (C, H, N and S) within the accepted experimental error. The errors were slightly higher for **F6** in the case of N, but not for the other elements. In the case of **F4** and **F5**, the errors were higher for S, C and H, which must be associated with the difficult combustion of the bulk IL, being this behaviour dependent on the nature of the counter anion [19]. All prepared membranes were transparent, flexible, and could be easily cut into any desired size and shape or be bent with one pair of tweezers, even under dry conditions (see Fig. 1). Interestingly, no appreciable leakage of the bulk IL was observed for polymers **F4**–**F6** even after a prolonged treatment with organic solvents. More than 95% of the IL remained in the SILLP-composite after Soxhlet extraction. For this experiment, the corresponding weighted samples were extracted with a good solvent for the corresponding IL (CH_2Cl_2) during 48 h in a Soxhlet equipment and weighted again after vacuum drying. No weight loss was detected and the chemical characterization provided the same results than for the initial polymers.

3.2. FT-Raman studies

Very small variations were observed in the FT-IR and RAMAN spectra for films of the first family (**F1**, **F2** and **F3**) and also very small variations were detected within the second family of films (**F4** and **F5**). The spectra obtained for **F6** were also very similar to those of **F4** and **F5**. However, more significant variations were observed when comparing both families of films, the one containing the IL absorbed in the matrix (**F4**–**F6**) and the other not containing such additive (**F1**–**F3**). Thus, for instance, Fig. 2 shows the partial RAMAN spectra obtained for **F2** and **F4**. It is interesting to note that for **F4** the band at 1630 cm^{-1} completely disappeared. This can be assigned to the absence of residual unreacted double bonds and is indicative of a higher degree of consumption of the polymerizable vinylic groups from **1**. Thus, the presence of the porogenic IL, along with the much lower crosslinking degree, most likely provides a higher degree of mobility to the growing polymeric chains and facilitates the reaction of all the double bonds of the trifunctional crosslinkers. On the other hand, the appearance of new bands at 1388, 627 and 606 cm^{-1} in **F4** is clearly visible, which can be assigned to the presence of [BMIM][NTf_2] absorbed in the polymeric matrix [20].

Besides, the morphology of the membranes could be further characterized by optical and Raman microscopy. Optical microscopy images (Fig. 3a) show that the surfaces of the films are not fully uniform and present some irregular patterns corresponding to areas protruding from the surface of the film.

However, a detailed study of these patterns through FT-Raman-mapping at several wavelengths, characteristic for the different components of the films (Fig. 3b and c), suggests a uniform and compact distribution of the components within the different regions. The same changes in intensity are observed between the regions for the different bands studied and, thus, seem to correspond to the above mentioned physical heterogeneity more than to changes in composition.

3.3. Differential scanning calorimetry studies

DSC curves were obtained for the different films at 10 K/min rate, under a nitrogen atmosphere, for the −70 to 80 °C range. The corresponding thermograms, registered after two initial heating and cooling cycles, are shown in Fig. 4a. In order to properly analyse the DSC curves, the bulk ILs involved in the preparation of films

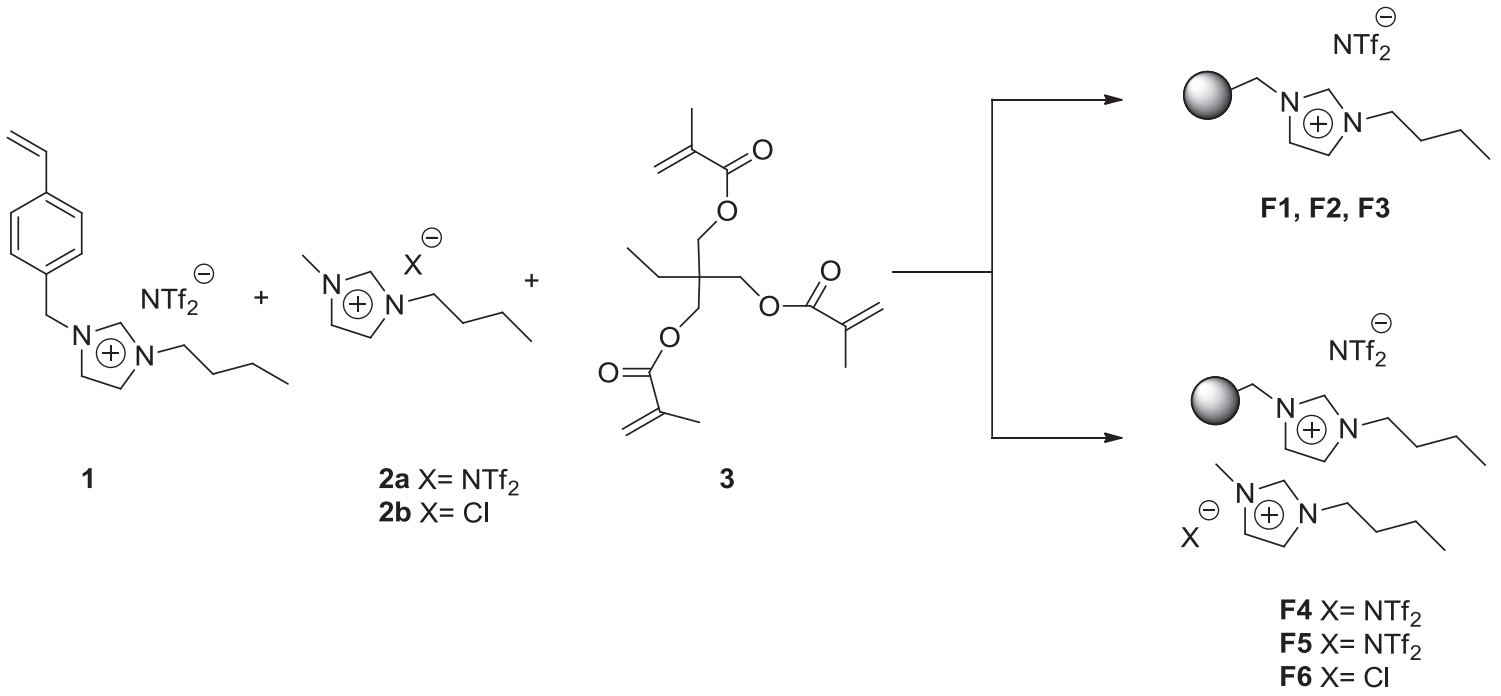

Scheme 1. Synthesis of films **F1**–**F6** (1% AIBN, 65 °C, 24 h).

Table 1
Chemical composition of the films and theoretical and experimental ion loading.

Entry	Film	Composition (% weight)			Exp. loading in mmol/g (theor. loading)		
		1	IL	3	1	IL	Total[c]
1	**F1**	60	–	40	1.1 (1.1)		1.1 (1.1)
2	**F2**	70	–	30	1.3 (1.3)		1.3 (1.3)
3	**F3**	87	–	13	1.6 (1.7)		1.6 (1.7)
4	**F4**	69	20[a]	11	– (1.3)	– (0.5)[a]	1.8 (1.8)
5	**F5**	58	34[a]	8	– (1.1)	– (0.8)[a]	1.8 (1.9)
6	**F6**	59	33[b]	8	1.1 (1.1)[c]	1.8 (1.9)[b]	2.9 (3.0)

[d]The experimental loading of **1** in film **F6** has been calculated from the data of %S experimental.
[a] IL **2a**.
[b] IL **2b**.
[c] The experimental total ion loading has been calculated from the data of %N experimental, the theoretical loadings according to the composition are given in parentheses.

F4–**F6**, namely [BMIM][NTf_2], **2a**, ([BMIM][Cl], **2b**, and the equimolecular mixture of both ILs were also studied under the same experimental conditions and the resulting DSC curves are presented in Fig. 4b.

As could be expected for crosslinked PS-DVB polymers, which do not possess detectable T_g values for the temperature range considered (−70 to 120 °C, according to the conductivity studies to be carried out), the curves obtained for **F1**–**F3** do not show appreciable transitions and present similar DSC curves, although some changes in the slopes are observed, due to the different chemical composition and crosslinking degree. The situation is clearly different for polymers **F4**–**F6** containing absorbed bulk ILs. To properly understand the thermograms obtained the DSC analyses for the corresponding bulk ILs used need to be considered. Fig. 4b gathers the DSC curves obtained for [BMIM][NTf_2], [BMIM][Cl] and an equimolecular mixture of both under similar experimental conditions than those used for the films. The DSC analysis for [BMIM][Cl], **2b**, was carried out, under the same experimental conditions used for the films, between −60 and 125 °C considering previous literature data [21]. The resulting curve was characterized by the presence of two well defined small endothermic peaks at ca. −47 and 63 °C in the heating ramp. These values show a good agreement with the values reported in the literature for the orthorhombic polymorph, taking into account the large influence of the purity of the samples and the conditions for their preparation and measurement [21d]. Thus, for instance, the presence of a glass transition at −48 °C and the melting at 68 °C has been described for this polymorph [21b]. As in other instances [21b], the melting associated to the second metastable polymorph (monoclinic) reported at temperatures ranging from 30 to 41 °C was not observed. The corresponding defined transitions were not clearly observable in the cooling ramp under our experimental conditions, a situation that is relatively common, although a small diffuse transition seems to be present below 70 °C and a glass transition is present below −50 °C. A T_g value of −69 °C has been calculated for this IL by Brennecke and coworkers [22]. For [BMIM][NTf_2], **2a**, the DSC analysis was carried out from −100 to 50 °C, taking into account its behaviour as a room temperature Ionic Liquid (RTIL) and the thermal properties described in the literature [23]. The less coordinating NTf_2^- anion affords a lower degree of structural organization and the corresponding curve does not allow, under our conditions, the observation, for the heating ramp, of the melting transition for which T_m values from −2 to −6 have been assigned [22,23]. In this heating ramp, however, a clear glass transition is present between −70 and −60 °C along with the observation of a minor transition at ca. −23 °C. The cooling ramp is characterized by a significant transition starting at ca. −25 °C and the presence of a small exothermic peak around −47 °C. For this IL (**2a**) a T_g value of −87 °C has been reported by different groups [22,23], while a cold crystallization (T_{cc}) at −44 °C has also been described [22]. Interestingly the well-defined structure observed for [BMIM][Cl], **2b**, is clearly lost in the equimolecular mixture with [BMIM][NTf_2], **2a**. This has been observed for different mixtures of ILs [21d]. In this case, no defined peaks are observed, although the curve is dominated by the low temperature transitions similar to those observed in the case of **2a**. In the case of **F4**, containing a 20% of **2a**, the observed DSC displays some significant differences with those of both polymers **F1**–**F3** and the bulk IL **2a**. A more ordered structure is detected as suggested by the glass transitions observed below ca. 30 and −25 °C (this one similar to the one observed for **2a**) in the cooling ramp and at ca. 40 °C in the heating ramp. No one of them is detected in the related **F1**–**F3**. In the case of **F5**, with a higher content of **2a** (34% instead of 20%) and a lower crosslinking degree (8% instead of 11%), the transition detected below 25 °C in the cooling ramp is much more important than the similar one detected for **F4**, while the ones at ca. −55 °C in the heating and cooling ramps are less well defined. The temperatures for these transitions are clearly different in **F5** and **2a** and the T_{cc} of the bulk IL at −47 °C is not detectable. As was observed in the case of the mixture of bulk ILs **2a**/**2b**, the presence of chloride and bistriflamide salts in the composite film **F6** is accompanied by a clear disruption of the partly ordered structures found in the cases of **F4** and **F5** and the DSC curve becomes very similar to these obtained for **F1**–**F3**. Overall, the presence of a single bulk IL, containing the same counter anion present in the SILLP, absorbed on the porous structure of the macroporous SILLPs studied in this work, could produce ordered monolayers of ILs deposited on the internal surfaces of the polymeric films. Such ordered structures seem to be absent, or at least significantly decreased, when the system is prepared in the presence of a mixture of counter anions for the SILLP and the bulk IL. Clearly this can have an important influence on the conductivity properties of these materials that are associated to the mobility of the corresponding ions.

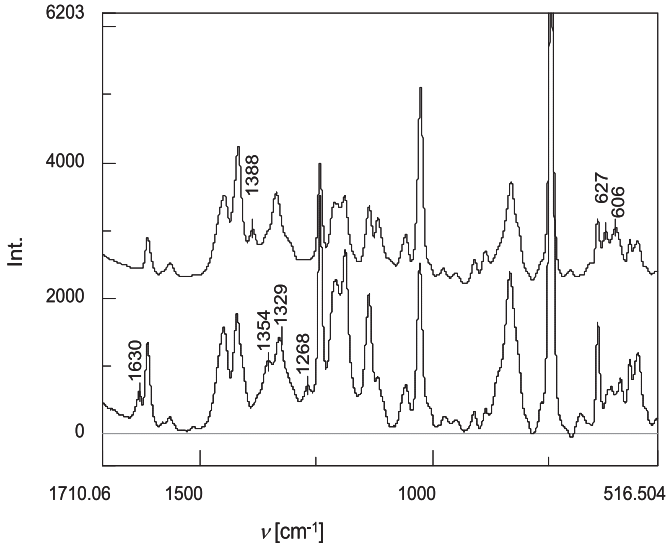

Fig. 2. Partial RAMAN spectra for the films **F4** (black line) and **F2** (grey line).

3.4. Electrochemical impedance spectroscopy

Electrochemical impedance spectroscopy (ISE) measurements were carried out for the samples $\mathbf{F_i}$ (i = 1, 2, 3, 4, 5 and 6) at different

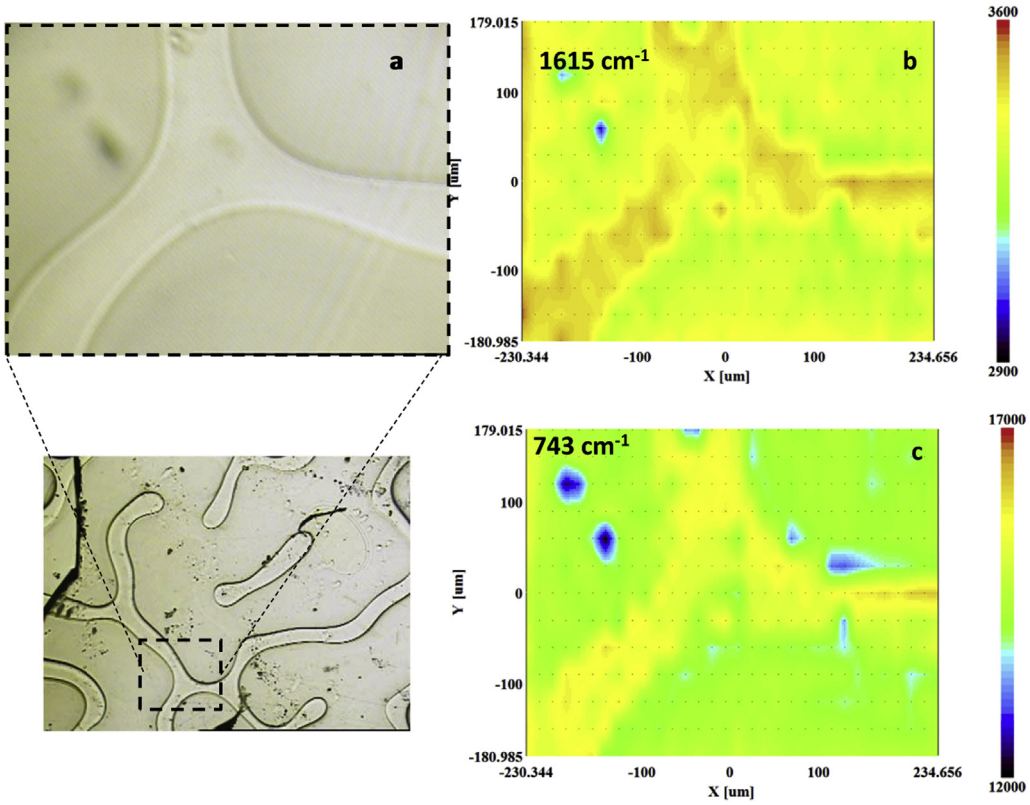

Fig. 3. Optical microscopy (a, 16×, bottom, × 32×, top) and FT-Raman mapping of a sample of **F4**. Mapping images b and c were obtained by measuring the intensity of the bands at 1615 (b) and 743 cm^{-1} (c).

temperatures in order to obtain information on their ion conductivity. The data were analysed in terms of their dielectric permittivity $\varepsilon^* = \varepsilon' - j\varepsilon''$, from which the imaginary part gives the conductivity (σ), as for a pure Ohmic conduction $\varepsilon'' = \sigma/(\varepsilon_0 w)$, where ε_0 represents the permittivity of vacuum and ω the angular frequency of the applied electric field. The real part of the conductivity (σ'), is characterized on the high frequency side by a plateau, the value of which directly yields the dc conductivity, σ_{dc}, and the characteristic radial frequency, $\omega_c = 2\pi f_c$, at which dispersion sets in and turns into a power law at higher frequencies. On the other hand, the real part of the dielectric function ε' at f_c turns from the high frequency limit to the static value ε_s. At lower frequencies, it is observed that σ' decreases from σ_{dc} and this is due to electrode polarization that results from blocking of charge carriers at the electrodes [24].

In Fig. 5 the double logarithmic plots of the real and imaginary permittivity and conductivity (ε', σ', ε'' and σ'') *vs.* the frequency are given for all the samples at 50 °C. From these figures we can observe three regions related with different behaviours of the samples: The low-frequency region of the spectrum is characterized by the electrode polarization (EP) where the formation of electrochemical double layers is satisfied. This frequency corresponds to the inflexion frequency in the double logarithmic plot of the real part of the conductivity (Fig. 5d). Note that at this frequency a peak or a shoulder is observed in the log ε'' *vs.* log f plot (Fig. 5b). This is a field of study of great interest in the case of ILs and related materials, such as the ones studied in this work, in order to explore their possible use as electrolytes for supercapacitors [25].

The region where a plateau regime is detected for the real part of the conductivity (Fig. 5d) corresponds with the bulk dc conductivity σ_{dc}, and, accordingly the conductivity of the SILLPs could be determined in this region, reflecting long-range ion transport. Finally, at higher frequencies, $\sigma'(\omega)$ increases with increasing frequency. In this region the subdiffusive conductivity (SD) is obtained and corresponds to a dispersive regime containing information of localized movements of ions in the electrolytes [26]. The analysis of this part of the spectra is, however, beyond the scope of this study.

From the log–log plot of ε' *vs.* frequency given in Fig. 5a at 50 °C of temperature, it can be observed that the dielectric strength increases with the loading of the IL-like fragments (BMIN [NTF_2] like units) covalently attached to the polymeric network. This is easily realized when comparing the samples **F1** and **F2** with **F3**, which contains the highest loading (87%) of IL-like fragments, in particular for lower frequencies. This increment is more pronounced in the case of films containing ILs absorbed in the matrix (**F4**, **F5** and **F6**). For **F4**–**F6** the values of the dielectric strength at lower frequencies follow the trend expected for the total content in IL fragments (bulk IL **2**+ monomeric IL **1**, see Table 1), while at higher frequencies the observed values follow the order associated to the content in bulk IL (**2**).

In general the dielectric strength follow the order **F1** < **F2** < **F3** < **F4** < **F5** < **F6**. This behaviour is not exclusive of this temperature but is maintained for the whole range of studied temperatures, indicating that the amount of transporting anion present is associated to an increasing of the strength.

As an illustration, the plots of log σ' and log σ'' *vs.* log f are shown in Fig. 6 for the sample **F6** for all the range of temperatures studied. The representation of both the real and the imaginary components for such a large frequency range allows to easily visualizing the presence of two different processes: charge transport for ca. 10^2–10^6 Hz, and electrode polarization (EP) occurring at lower frequencies. It can be observed that the electrode polarization (EP) and the bulk charge transport are strongly dependent on the temperature. A similar behaviour was found for the other samples

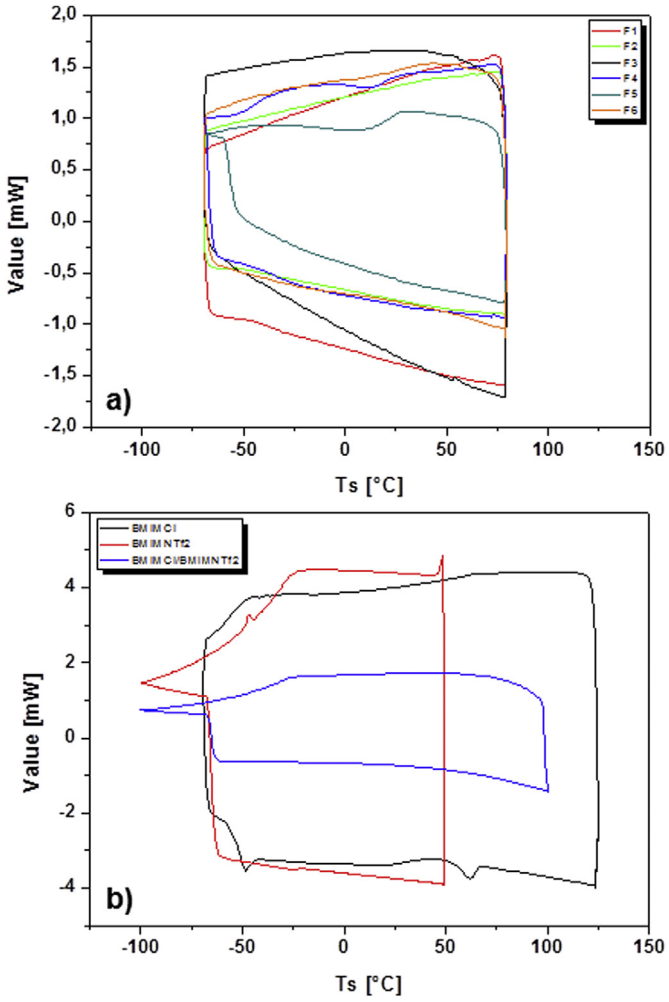

Fig. 4. (a) DSC thermograms for the films **F1**–**F6**; (b) DSC thermograms for ILs **2a**, **2b** and an equimolecular mixture of both.

F$_i$ (i = 1, 2, 3, 4, 5). Such performance has also been found in bulk imidazolium ionic liquids by other researchers [27].

A close inspection of data in Fig. 5a, corresponding to the double logarithmic plot of log ε' *vs.* log f for **F6**, shows that, at high frequencies, in the range 10^6 Hz–10^7 Hz range, $\varepsilon'(\infty) \cong 17$. This observed value is slightly higher than those reported as typical for many ionic liquids and glasses whose conductivity is characterized by the mobility of NTf_2^- ions, where the value of permittivity varies between 6 and 11 at 50 °C [28]. The static dielectric permittivity values calculated by dielectric relaxation spectroscopy for a series of dialkylimidazolium bistriflamides at 25 °C ranged between 12 and 15, being of the same order for other aprotic ILs and much higher for protic ILs [29]. It is worth mentioning that in our case the calculated dielectric constants range from 6 to 17 at 50 °C, the observed value being very similar for films **F1**–**F3**, but clearly higher for the films **F4**–**F6** containing absorbed bulk ILs.

For this dielectric constant range, the Bjerrum length is about 3 nm. In this situation several rearrangements of neighbouring fragments and ions must take place and this value is presumably the dielectric constant more relevant to analyse the potential use of the developed materials in a macroscopic capacitor. In the case of the films studied in this work, the trend observed for the values of the static permittivity (**F1** < **F2** < **F3** < **F4** < **F5** < **F6**) is clearly related to their chemical composition. The corresponding values range from 6 (**F1**) to 17 (**F6**). The dielectric relaxation strength $\varepsilon'(0)$–$\varepsilon'(\infty)$, is a measure for the dipole fluctuation due to fast processes, and from there the mean square displacement of the anions in the samples **F1**–**F6** can be estimated according the following equation [26b].

$$\left\langle \tilde{R}^2(\infty) \right\rangle_{cr} = \frac{6k_B T\varepsilon_0}{N_v q^2}[\varepsilon'(0) - \varepsilon'(\infty)] \quad (1)$$

where q is the ionic charge, ε_0 denotes the permittivity of the free space, N_v the average number density of the charges (for simplicity, N_v for NTf_2^- has been used for all cases, assuming that NTf_2^- is the most relevant anion for all the samples). From Eq. (1) values ranging from 4 to 7 Å were obtained for the mean square displacement of the anions. These values are close to the diameter calculated for the imidazolium cations and the NTf_2^- anions, and very close to the values observed by Huber et al. [30].

When normalizing the results with respect to the dc conductivity (σ_{dc}) and the electrode polarization frequency f_c, it is remarkable that a coinciding plot is obtained for all the samples for the whole range of temperatures studied, as illustrated in Fig. 6 for **F6**. As seen in Fig. 6 (bottom graphs) the isotherms superpose rather well over the isotherm of reference. Notice that the master curve extends over roughly 10 decades. Similar results are found for the other samples. This implies the existence of a single charge transport mechanism for all the samples studied in this paper.

From the Bode diagram [31] shown in Fig. 6 (left graphic on the top) for the sample **F6**, the conductivity of the sample at all the studied temperatures can be obtained. The pertinent results are given in Table 2. In Fig. 7, the values of the conductivity for all the samples as a function of the temperature are represented. The data show a Vogel–Fulcher–Tamman-type behaviour, which is typical for the majority of polymers at temperatures above T_g. For all temperatures studied the values of σ increase with the temperature, following the order σ(**F6**) > σ(**F5**) > σ(**F4**) > σ(**F3**) > σ(**F2**) > σ(**F1**). As observed in Fig. 7, the dc conductivity increases when the amount of the crosslinker (**3**) decreases, as this is associated simultaneously to a higher mobility of the polymeric chain and to an increase in the loading of IL-like fragments covalently attached to the polymeric matrix. On the other hand, when the amount of the bulk IL (**2a**) increases from 20% (**F4**) to 34% (**F5**) the conductivity also increases. For example, at 50 °C the value changes from 2.3×10^{-5} S/cm for **F4** to 6.6×10^{-5} S/cm for **F5**. Taking into account that the total loading of imidazolium units (mmol/g, considering both the bulk IL **2a** and the fragments covalently attached originating from **1**) is very similar for **F4** and **F5**, these results indicate a clearly higher contribution to the final conductivity from the bulk IL. This is also in good agreement with the significant differences observed in conductivity between **F3** and **F4**, differing less in total loading than **F2** and **F3**. Finally, when the ion NTf_2^- in the component **2a** is replaced by the anion Cl^- (component **2b**) the dc conductivity increases further, for the same loading and crosslinking degree, reaching a conductivity value of 1.9x10-3 S/cm for **F6** at 100 °C. A general comparison between all the samples for the whole range of temperatures shows, for instance, that the dc conductivity of **F6** increases from 8.25×10^{-6} S/cm at 0 °C to 3.5×10^{-3} S/cm at 130 °C, while in case of the sample **F1** this increase is from 9.1×10^{-11} S/cm to 1.84×10^{-5} S/cm for the same temperature range. As can be observed, this represents a huge increase in conductivity, in particular at low temperatures (up to 5 orders of magnitude) obtained through a proper selection of the overall components and structure of the corresponding SILLP films.

As seen in Fig. 7, the addition of 20% in weight of the IL component **2a** containing the NTf_2^- anion, produces an increase of two orders of magnitude in the conductivity for all the range of temperatures with respect to the samples **F1**, **F2** and **F3** obtained from different monomeric mixtures but not containing any bulk IL.

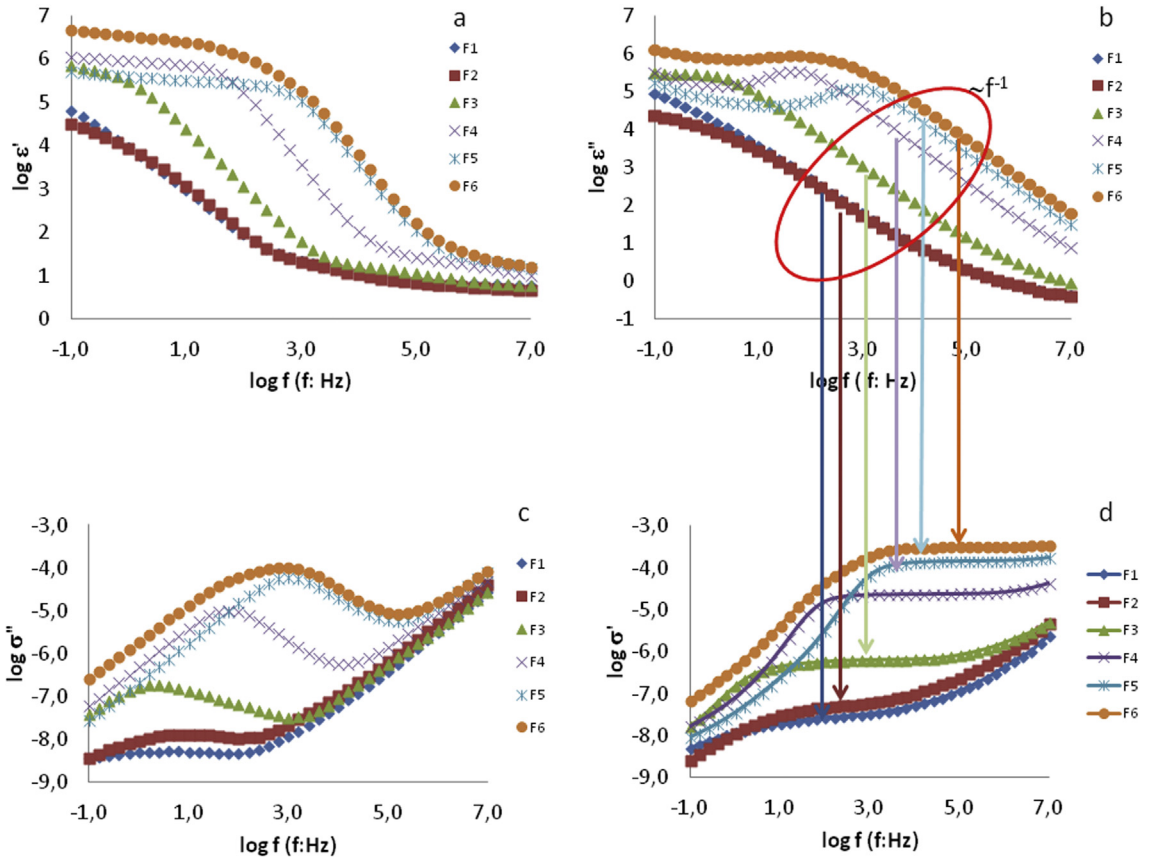

Fig. 5. Double logarithmic plots of the real and imaginary permittivity and conductivity (ε', σ', ε'' and σ'') *vs.* frequency for all the samples at 50 °C.

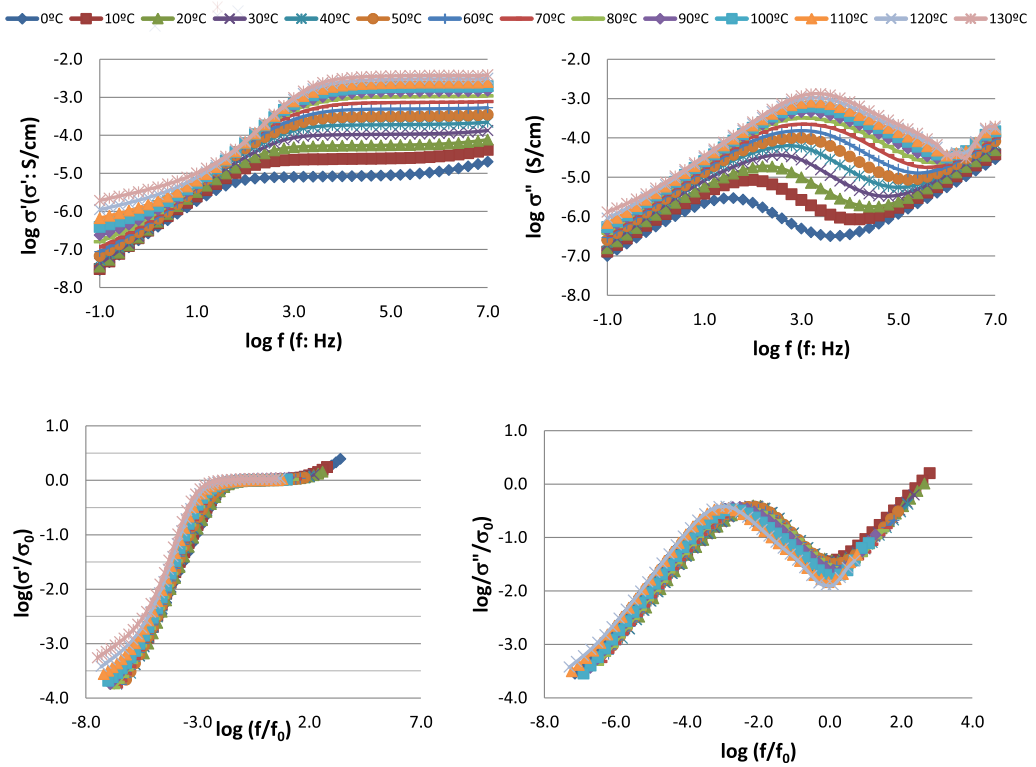

Fig. 6. General behaviour of the sample **F6** at different temperatures. (Top): double logarithmic plots of σ' and σ'' *vs.* frequency. (Bottom): master curve of the normalized plots respect to the real and imaginary parts of the conductivity.

Table 2
Conductivity values obtained from the Bode diagrams for all the SILLPs at the different temperatures studied.

T (°C)	**F1** σ(S/cm)	**F2** σ(S/cm)	**F3** σ(S/cm)	**F4** σ(S/cm)	**F5** σ(S/cm)	**F6** σ(S/cm)
20	3.1×10^{-10}	3.5×10^{-10}	9.8×10^{-10}	1.5×10^{-6}	2.1×10^{-5}	5.4×10^{-5}
40	6.0×10^{-9}	6.4×10^{-9}	7.9×10^{-9}	1.2×10^{-5}	8.3×10^{-5}	1.7×10^{-4}
60	8.4×10^{-8}	9.0×10^{-8}	1.9×10^{-6}	4.4×10^{-5}	2.3×10^{-4}	4.5×10^{-4}
80	6.1×10^{-7}	6.3×10^{-7}	9.7×10^{-6}	1.3×10^{-4}	5.1×10^{-4}	9.0×10^{-4}
100	3.1×10^{-6}	3.4×10^{-6}	3.5×10^{-5}	2.7×10^{-4}	9.9×10^{-4}	1.9×10^{-3}
120	1.0×10^{-5}	1.1×10^{-5}	8.5×10^{-5}	5.2×10^{-4}	1.2×10^{-3}	2.9×10^{-3}

When the amount of NTf_2^- anion increases to 34%, sample **F5**, the conductivity further increases, being almost three times higher for **F5** than for **F4**. Finally, when the anion of the bulk IL changes from NTf_2^- to Cl^-, the conductivity still increases two times, (see Table 2). These changes can clearly be related with the modification observed above in the thermal behaviour of these composites and the corresponding degree of ordering. It is interesting to compare the present results with those obtained, for instance, for a linear ABA triblock copolymer poly(styrene-b-[1-ethyl-3-(4-vinylbenzyl) imidazolium bis(trifluoromethane sulfonyl)imide)]-b-styrene) for which a value of ca. $5 \cdot 10^{-7}$ S cm^{-1} is observed around 40 °C, reaching a maximum measured value of about $3 \cdot 10^{-4}$ S cm^{-1}around 150 °C [32]. Taking into consideration the important changes in polarity and hygroscopicity associated to the change in the anion from NTf_2^- to Cl^- [8a], the presence of retained water could have an influence on the conductivity observed. Although the experimental protocol used was set-up to eliminate the water present in the composites, by carrying out an initial cycle (0 °C to 130 °C to 0 °C) before each measurement, this effect cannot be completely ruled out, if water molecules strongly associated to the IL fragments are present. On the other hand, it is also important to consider the changes often observed for the properties, including conductivity, of mixtures of ILs that can clearly deviate from linearity [33].

A close inspection of the variation of the values represented in the activation plot of Fig. 7 allows obtaining the temperature dependence of the charge transport values, according to the Vogel–Fulcher–Tammann equation

$$\log \sigma = \log \sigma_\infty - \frac{B}{T - T_0} \quad (2)$$

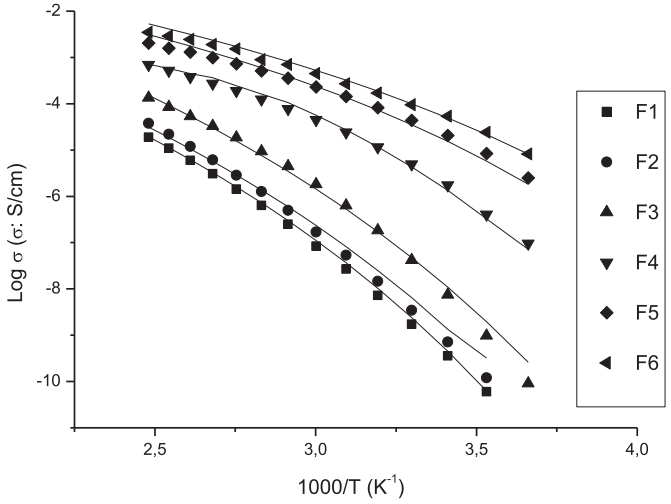

Fig. 7. Representation of the conductivity as a function of the reciprocal of the temperature for all the samples studied. The solid line represents the fit to a Vogel–Fulcher–Tammann behaviour.

where B is a fitting parameter related with the curvature of the plot that can be seen as the high temperature activation energy of the process underlying the conductivity σ_{dc}. T_0 is the Vogel temperature, considered as the one at which the relaxation time would diverge and σ_∞ is a pre-factor related with the limit conductivity at higher temperatures. In Table 3 the corresponding values obtained for the parameters σ_∞, T_0 and B are gathered. In the same table the values found for the activation energy have also been tabulated.

The values of the activation energy follow the trend **F1** > **F2** ≈ **F3** > **F4** ≈ **F5** > **F6** being in most cases smaller than the values obtained for imidazolium-based ionic liquids in aqueous solutions, where the activation energy was about 19 kJ/mol [34]. This indicates that excellent ion mobilities can be obtained with these films in comparison with the aqueous solutions of similar ILs. The comparison of **F1** and **F2** reveals that a decrease in the crosslinking with the associated increase of the IL-like loading, and accordingly the improvement in the mobility of the polymeric chains and the attached functional groups, is clearly accompanied by a decrease in E_{act}. However, this effect seems to reach a limit for a value of crosslinking around 30%, as a further decrease up to 13% in **F3** (and the increase in IL-like fragments loading from 1.3 to 1.6 mmol/g) is not accompanied by a significant decrease in the value of E_{act}. The incorporation of bulk ILs to the composite films is associated to a larger decrease in E_{act} than those observed for the changes in the monomeric composition. Thus, **F4** and **F5** show E_{act} values that are half than those for **F3**. However, the increase in the amount of the IL **2a** from 20% to 34% is not accompanied by an appreciable decrease in this parameter. On the other hand, the exact nature of the IL, and particularly the nature of the anion, is critical. Changing the anion from NTf_2^- to Cl^-, using **2b** in **F6**, produces a further decrease in E_{act} by about 10%. As expected, these results are in excellent agreement with the values obtained for the dc conductivities.

3.5. Diffusion coefficients and charge concentration

In binary salt/polymer solutions both anions and cations can be mobile, since most of them may be interacting forming ion pairs or clusters. According to this, the concentration of the mobile charges involved can be difficult to calculate. However, the total concentration of the charge carrier can be estimated following the procedure described by Sorensen and Compañ [35], limiting the generalization of the Trukhan model based on the Nernst–Planck equations of electrodiffusion, where the electrolyte considered is a

Table 3
VFT fitting parameters for the supported ionic liquids (SILLPs) studied in this work.

Entry	Sample	Ln σ_∞ (S/cm)	B × 10^{-3} (K)	T_0 (K)	E_{act} (kJ/mol)
1	**F1**	1.0 ± 0.05	2.89 ± 0.02	167 ± 1	24.0 ± 0.1
2	**F2**	0.80 ± 0.02	2.87 ± 0.02	165 ± 1	23.9 ± 0.1
3	**F3**	2.20 ± 0.05	2.70 ± 0.02	162 ± 1	22.4 ± 0.1
4	**F4**	0.50 ± 0.02	1.80 ± 0.01	165 ± 1	15.0 ± 0.1
5	**F5**	0.12 ± 0.02	1.47 ± 0.01	161 ± 1	12.2 ± 0.1
6	**F6**	0.18 ± 0.02	1.36 ± 0.01	160 ± 1	11.3 ± 0.1

binary system and the diffusion coefficients in the same phase may be different [36,37]. This approach has also been used to model the electrode polarization in the case of ionomers with anions fixed along the polymer chains and the cations as mobile counterions [38]. This is clearly a good model for the systems here considered, as the samples under study contain ionomers with cations fixed along the polymer chains and anions like NTf_2^- or Cl^- can move easily along the polymer.

The model allows to make an estimation of the diffusion coefficients and the concentration of the free charge (mobile ion) carriers from the values of the maximum of loss tangent (tan δ), where δ is the phase angle of the complex dielectric permittivity, ε^*. Assuming a 1:1 stoichiometry for the electrolyte, with equal diffusion coefficients, and the film to be "thick" compared with the Debye length, the diffusion coefficients for the anion, D_a, and cation, D_c, ($D_a = D_c$) can be estimated according to Eq. (3) [35–37,39].

$$D = \frac{2\pi}{32}\frac{f_{max}\cdot L^2}{[(\tan\delta)_{max}]^3} \quad (3)$$

where f_{max} is the value of the frequency corresponding to the maximum of the loss tangent, L is the thickness of the sample and $(\tan\delta)_{max}$ the value of the loss tangent at the maximum of the spectrum. When the Maxwell–Wagner–Sillars (MWS) effects dominate completely over the effects of the surface polarization at low frequencies and the internal relaxations in the polymer (moderate and high frequencies) are present, then the plot of log (ε'') *vs.* log *f* yields a straight line with slope −1 over an extended range of intermediate frequencies (see Fig. 5b). This is a clear indication of a MWS behaviour and from the intersection of this line with log *f* = 0 we can estimate the conductivity. Identically, in the plot of the log (σ') *vs.* log *f* a plateau is observed in the same range of frequencies for which log (ε'') *vs.* log *f* displays a straight line with slope −1. From this plateau we could obtain the dc-conductivity and the pertinent results following this procedure were presented in Table 2.

Fig. 8 shows the values of tan δ as a function of the perturbation frequency, at 50 °C, for all the samples studied. Well defined single maxima in tan δ appearing at different frequencies in each case, can be observed. The frequency for the appearance of such a maximum is dependent on the working temperature as is illustrated in the inset of the figure displaying the results found for **F4** in all the range of temperatures. A similar behaviour has been observed for the other SILLPs. As can be seen in the inset for the sample **F4**, the relaxation strength increases slightly with temperature and as the temperature increases the frequency of the maximum shifts to higher values. The same trend is also detected for the other samples.

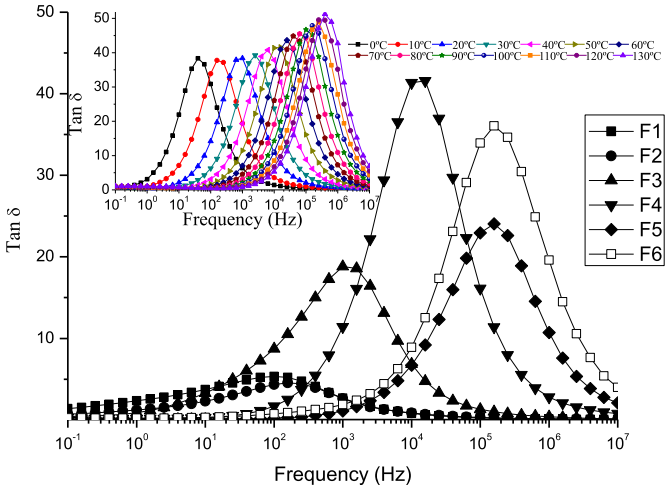

Fig. 8. Representation of tan δ *vs.* frequency for **F1**–**F6** at 50 °C The inset shows the temperature dependence of this plot for **F4** (from 0 °C to 130 °C).

As observed in Fig. 8, the intensity and the frequency of the peaks is very sensitive to the different structural elements present in the SILLPs and composites studied. Thus, both the intensity and the frequency of the peak are quite similar for **F1** and **F2** even if the loading of covalently attached ionic fragments for the second is higher (70% of imidazolium monomer **1** instead of 60% or 1.3 *vs.* 1.1 mmol/g) and, accordingly, the crosslinking is lower (30% of monomer **3** instead of 40%). However, a large increase in the value of tan δ, from ca. 5 to ca. 20, is observed for **F3** in which the loading has increased to 1.6 mmol/g (87% of monomer **1**) and the crosslinking decreased to 13%. The position of the maximum is concomitantly shifted to higher frequencies. This seems to suggest that there is minimum value of loading or a maximum value of crosslinking (or both) required to reach significant values of tan δ. An additional increase in diffusivity to a value of ca. 40, and an accompanying shift to higher frequencies, is observed for **F4** where the covalently attached IL-like fragments of **F3** are partly substituted by a related bulk IL (**2a**), which maintains almost unchanged the crosslinking degree but increases the molar loading of the film from 1.6 to 1.8. Rather surprisingly, a further increase in the percentage of the bulk IL absorbed in the SILLP, but maintaining constant the total ion loading in 1.8 mmol/g, giving place to **F5**, is not accompanied by an additional increase in the maximum value of tan δ. On the contrary this value is reduced to ca. 25, although the frequency of the maximum is still shifted to higher values. This could be associated to appreciable changes in relaxation times. Interestingly the change of the NTf_2^- counter anion for Cl^- also has an effect. Thus, **F5** and **F6** only differ in their weight composition in the fact that **F5** is prepared using **2a** (NTf_2^- counter anion) as the porogenic bulk IL, while **2b** (Cl^- counter anion) is used for **F6**. This leads to a modification of the anions present and to an increase in the total ion loading (2.9 *vs.* 1.8 mmol/g). A significant increase in the maximum value of tan δ is observed for **F6** (from ca. 25 to ca. 35) although no shift in the frequency is observed.

The inset in Fig. 8 shows the temperature dependence of tan δ for **F4** from 0 °C to 130 °C that reveals that the relaxation strength increases slightly with temperature. On the other hand, the representation of the electrode polarization time τ_{EP} as a function of the reciprocal of the temperature (Fig. 9) presents a curve that, in general, cannot be described through a simple Arrhenius fit, indicating that in the considered SILLPs and composites a simple dependence with the temperature is not present. Taking into account that τ_{EP} represents the mean time for an ion to travel from one electrode to another, at times longer than τ_{EP} a large quantity of mobile ions will have built up at the electrodes and the dependence with temperature of ion mobilities will not present an Arrhenius behaviour, as will happen with the conductivity (see Fig. 7). Similar results have been found for poly(ethylene oxide) based sulfonated ionomers having different cations such as Li^+, $Na^+$and Cs^+ [36]. As can be see in Fig. 9, the polarization times increase with the decrease in the loading of IL-like fragments (compare, for instance samples **F1** and **F3**). Nevertheless, the most critical factor seems to be the presence of bulk ILs absorbed on the polymeric matrix. In general, the presence of bulk ILs produces a decreasing of the values of τ_{EP} that can be up to 2–3 orders of magnitude smaller for **F4**–**F6** than for **F1**–**F3** at the same temperature. Comparing **F4** and **F5** reveals that an increase in the amount of absorbed IL produces an additional decrease in the polarization times, in particular at lower temperatures, with the corresponding values converging at high temperatures. The comparison between **F5** and **F6** suggests

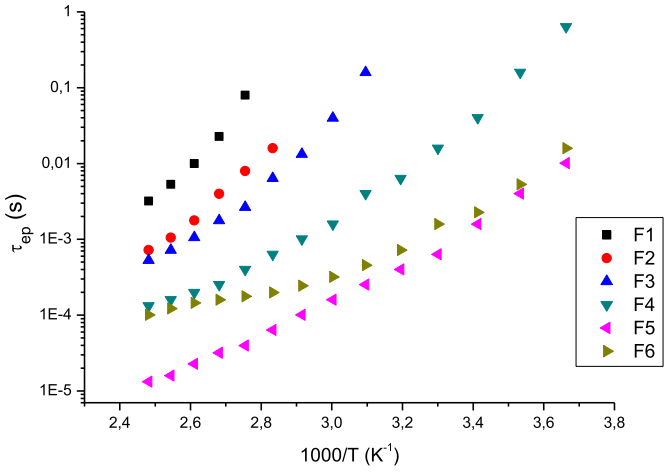

Fig. 9. Temperature dependence of the electrode polarization time τ_{EP}.

that the change in the counter anion of the bulk IL from NTf_2^- to Cl^- is not significative at low temperatures but above ambient temperature, the polarization times decrease more rapidly for **F6** than for **F5**, which suggests that the counter anion of the bulk IL affects the frequency at which the polarization starts to be present in the system and, accordingly, is affected by its chemical nature.

From the data previously obtained, and using the Eq. (3), the diffusion coefficients for the different SILLPs can be obtained as a function of the temperature. The corresponding plots are presented in Fig. 10. From the analysis of our results it can be observed that the diffusion coefficients can be very much affected by different structural parameters of the films. This is particularly evident at lower temperatures, where the corresponding coefficients can differ by almost 5 orders of magnitude. In all cases, the diffusion coefficients increase with the temperature, but this effect is more pronounced for samples **F1**–**F3** having solely ionic fragments with the cations covalently attached to the polymeric network. In this case, the diffusion observed must involve the hoping of the anions and can have a significant contribution from the dynamic of the polymeric chains. From the results we can see that the most remarkable effect of the temperature is observed for **F3**, the polymer of this family containing the lower crosslinking degree and the higher loading of ionic fragments. Thus, these changes with temperature seem to reflect the increased mobility of the polymeric chains containing the ionic groups. The presence of bulk ILs absorbed on the polymeric matrix seems to reduce the effect of the temperature on the diffusion coefficients. This suggests that, in these cases, the contribution of the bulk IL to the diffusion coefficients is predominant. For most of the temperature range studied, except for the higher temperatures, **F5** and **F6**, the polymers containing a larger amount of bulk IL, are the films displaying higher values of the diffusion coefficients. It must be noted that the curves for **F5** and **F6** are very similar, although the values for **F5** are always slightly higher than those for **F6**. Although the weight composition of both composites is similar (Table 1) the total ion loading for **F6** is significantly higher (2.9 *vs.* 1.8 for **F5**) and this corresponds to a higher molar loading of the bulk IL (1.9 mmol/g *vs.* 0.8 mmol/f for **F5**). Accordingly, one could expect the reverse trend in the observed values of the diffusion coefficients, with the values for **F6** being constantly higher. Thus, the nature of the anion in the bulk IL (NTf_2^- in **F5** and Cl^- in **F6**) seems to play an important role for this parameter.

The measured conductivity is the sum of the total contributions of the charge carriers, cations and anions, assuming that all the available ions participate in the ionic transport. From the experimental results we have estimated the total conductivity and its value can be associated to the maximum possible contribution of the cations [40]. The ionic conductivity is related with the diffusion coefficient and the mobile ion concentration, c_{ion}, by the Eq. (4), [32–34,36].

$$\sigma_{dc} = \frac{F^2}{R \cdot T \cdot N_A} c_{ion} D \tag{4}$$

In this equation, σ_{dc} represents the ionic conductivity determined from the Bode diagrams [31] obtained from the dielectric spectra at the frequency where the tangent of the dielectric loss angle presents a maximum, (i.e. the dc-conductivity), as is shown in Fig. 5, D is the diffusion coefficient obtained following the procedure described above, R is the gas constant, F is the Faraday constant, N_A the Avogadro number and T the absolute temperature. Using this equation, the theoretical charge carrier density (i.e. free ion concentration) in the samples, as a function of the temperature, can be estimated. The corresponding results are represented in Fig. 11. The results obtained show that the lower charge carrier density corresponds, as could be expected, to the films containing solely imidazolium subunits covalently attached to the polymeric matrix (**F1**–**F3**). As was discussed in the case of the tan δ values, **F1** and **F2** present a very similar

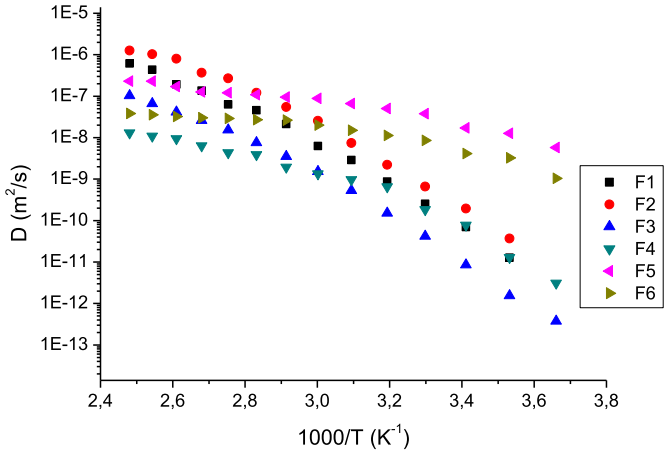

Fig. 10. Arrhenius plots for the diffusion coefficients obtained according the Truham model (Eq. (3)) for the different SILLPs.

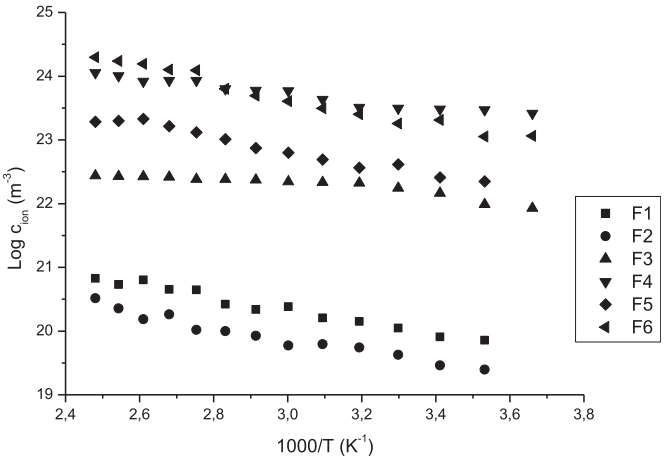

Fig. 11. Variation of the charge carrier density of the mobile ion *vs.* the reciprocal of the temperature for all the samples studied.

behaviour, while **F3** having a higher loading of ionic fragments and a lower crosslinking degree presents values for this parameter that are 1–2 orders of magnitude higher than those for **F1**–**F2**. The presence of absorbed bulk ILs is associated to an increase in the charge carrier density. A comparison between **F4** and **F5** shows that the increase from 20% to ca. 30% in the amount of bulk IL (**2a**), keeping essentially constant the total loading of IL-units, is accompanied by an increase of the values of about 1 order of magnitude. Very interestingly, for **F6**, structurally similar to **F5** but having Cl^- instead of NTf_2^- as the counter anion of the bulk IL (**2b**), the calculated charge carrier density is smaller than that for **F5**. This must be associated to the lower dissociation degrees present in **F5** according to the more coordinating nature of the Cl^- anion. It must also be noted that while **F1**–**F2**, and **F4**–**F6** display a clear variation of the values obtained with the temperature, they are almost invariable for **F3** for the whole temperature range studied.

4. Conclusions

Films prepared from SILLPs represent a very useful approach for conductive membranes. Significant conductivities can be achieved through a fine tuning of the structure of the SILLP, in particular when bulk ILs are incorporated as porogens that become strongly associated to the functional polymeric surfaces and do not leach under a variety of conditions (>95% retained after Soxhlet extraction). Both, the nature and degree of the crosslinking and the loading and structure of the IL moieties and the bulk IL, in particular the nature of the anion, are key parameters to understand the conductivities obtained.

It is important to note that the present approach, involving the polymerization of a styrenic imidazolium derivative and other(s) comonomer(s), including the corresponding crosslinking agents, in the presence of a bulk IL acting as the porogenic agent allows the preparation of composites based in polymers with relatively high crosslinking degrees (ca. 10%). In comparison with other approaches requiring polymers only lightly crosslinked, this allows the preparation of materials with good mechanical properties (i.e. mechanical stability, flexibility, shape persistence, etc) but, at the same time, providing excellent conductivity parameters that can be compared with those determined for bulk ILs. In this regard, conductivities reported at room temperature for bulk ILs can be up to two orders of magnitude higher than those obtained in our composites. Thus, for BMIM $[NTf_2]$ a value of $3.9\cdot10^{-3}$ S cm^{-1} has been reported [39,41], and a value of $0.25\cdot10^{-3}$ S cm^{-1} has been calculated for BMIM [Cl] at 40 °C. For the corresponding composites containing BMIM $[NTf_2]$ (**F4** and **F5**), conductivities at 20 °C are $0.15\cdot10^{-5}$ and $0.54\cdot10^{-4}$ S cm^{-1} respectively. Remarkably, for the composite (**F6**) containing BMIM [Cl] at 40 °C the value obtained is $0.17\cdot10^{-3}$ S cm^{-1}, which is almost identical to the value for the related bulk IL. It is important also to note that very important increases in conductivity can be achieved with a moderate increase in temperature. In this way, at 80 °C, the conductivity values for **F4**–**F6** increase 1–2 orders of magnitude relative to those at room temperature.

Besides, this can be achieved just using a limited amount of bulk IL (ca. 20–30%) in the preparation of the corresponding composites. The conductivity values achieved at operational temperatures for IL-SILLP based composites (**F4**–**F6**) compare well with those reported for other IL/polymer and IL/PIL blends and those observed for many proton exchange membrane fuel cell (PEMFC) polymeric electrolytes and other electrolytic systems for electrochemical devices such as supercapacitors and batteries [3]. This opens the way to the study of these materials, under the appropriate conditions allowing practical ionic conductivities, for this purpose. An illustrative comparison can be made with values reported for the non-crosslinked benchmark PIL poly(1-vinyl-3-ethylimidazolium) $[NTf_2]$ for which different studies have reported values of $6.3\cdot10^{-7}$, $2.5\cdot10^{-11}$ and $5.0\cdot10^{-5}$ S cm^{-1} at 20–30 °C [42], or with the related polystyerene derived PIL poly(styrene-b-[1-ethyl-3-(4-vinylbenzyl) imidazolium bis(trifluoromethane sulfonyl)imide)]-b-styrene) (ca. $5\cdot10^{-7}$ S cm^{-1} at ca. 40 °C) [32]. In general, high loadings of bulk ILs, ranging from 40% to 200%, are required to obtain acceptable conductivities, even in IL/PIL composites, in particular for crosslinked polymers [42c,43]. These high IL-loadings, however, compromise the mechanical stability and the practical applicability of many of those systems as solid electrolytes. This is not the case of the composites here considered, which, as mentioned, can be prepared as crosslinked polymeric PILs with good mechanical properties containing moderate amounts of bulk ILs. The results here presented reveal that a fine tuning of the properties of these SILLP-based polymeric composites is possible through an appropriate design of the different structural parameters. The modular nature of these structural parameters at both the polymeric matrix and the bulk IL greatly facilitates the corresponding optimization process and opens the way to the preparation of new families of conductive polymeric materials for further applications in different fields, in particular in energy-related areas.

Acknowledgements

Financial support by Ministerio de Ciencia e Innovación (CTQ2011-28903-C02-01 and SP-ENE-20120718), Generalitat Valenciana (PROMETEO/2012/020) and Universitat Jaume I (P11B2013-38) is acknowledged.

References

[1] (a) J.P. Hallett, T. Welton, Chem. Rev. 111 (2011) 3508;
(b) T. Welton, Chem. Rev. 99 (1999) 2071.
[2] M.P. Singh, R.K. Singh, S. Chandra, Prog. Mater. Sci. 64 (2014) 73.
[3] M. Diaz, A. Ortiz, I. Ortiz, J. Memb. Sci. 469 (2014) 379.
[4] N. Nishimura, H. Ohno, Polymer 55 (2014) 3289.
[5] (a) J. Yuan, D. Mecerreyes, M. Antonietti, Progr. Polym. Sci. 38 (2013) 1009;
(b) J. Yuan, M. Antonietti, Polymer 52 (2011) 1469;
(c) M.D. Green, T.H.E. Long, Polym. Rev. 49 (2009) 291.
[6] S.V. Luis, E. García-Verdugo, M.I. Burguete, A. Andrio, S. Molla, V. Compañ, Polymers with ionic liquid fragments as potential conducting materials for advanced applications, in: S. Handy (Ed.), Applications of Ionic Liquids in Science and Technology, InTech, 2011, pp. 83–108 (Chapter 5).
[7] S. Washiro, M. Yoshizawa, H. Nakajima, H. Ohno, Polymer 45 (2004) 1577.
[8] (a) V. Sans, N. Karbass, M.I. Burguete, V. Compañ, E. García-Verdugo, S.V. Luis, M. Pawlak, Chem. Eur. J. 17 (2011) 1894;
(b) A. Garcia-Bernabe, V. Compañ, M.I. Burguete, E. García-Verdugo, N. Karbass, S.V. Luis, E. Riande, J. Phys. Chem. C 114 (2010) 7030;
(c) V. Compañ, S. Molla, E. García-Verdugo, S.V. Luis, M.I. Burguete, J. Non-Cryst. Solids 358 (2012) 1228.
[9] (a) M.I. Burguete, F. Galindo, E. García-Verdugo, N. Karbass, S.V. Luis, Chem. Commun. (2007) 3086;
(b) N. Karbass, V. Sans, E. Garcia-Verdugo, M.I. Burguete, S.V. Luis, Chem. Commun. (2006) 3095. Phys. Chem. Chem. Phys. 13 (2011) 14831.
[10] J. Tang, H. Tang, W. Sun, M. Radosz, Y. Shen, J. Polym. Sci. A Polym. Chem. 43 (2005) 5477.
[11] H. Tang, J. Tang, S. Ding, M. Radosz, Y. Shen, J. Polym. Sci. A Polym. Chem. 43 (2005) 1432.
[12] J.E. Bara, C.J. Gabriel, E.S. Hatakeyamaa, T.K. Carlisle, S. Lessmann, R.D. Noble, D.L. Gin, J. Memb. Sci. 321 (2008) 3.
[13] D. Mecerreyes, Progr. Polym. Sci. 36 (2011) 1629.
[14] (a) A.S. Shaplov, D.O. Ponkratov, P.S. Vlasov, E.I. Lozinskaya, I.A. Malyshkina, F. Vidal, P.-H. Aubert, M. Armand, Ya. S. Vygodskii, Polym. Sci. Ser. B 56 (2) (2014) 164;
(b) A.S. Shaplov, D.O. Ponkratov, P.S. Vlasov, E.I. Lozinskaya, L.I. Komarova, I.A. Malyshkina, F. Vidal, G.T.M. Nguyen, M. Armand, C. Wandrey, Y.S. Vygodskii, Polym. Sci. Ser. B 55 (3–4) (2013) 122.
[15] D.F. Izquierdo, M. Yates, P. Lozano, M.I. Burguete, E. García-Verdugo, S.V. Luis, React. Funct. Polym. 85 (2014) 20.
[16] (a) J.-I. Kadokawa, M.-A. Murakami, Y. Kaneko, Compos. Sci. Technol. 68 (2008) 493;
(b) K. Prasad, S. Mine, Y. Kaneko, J.-I. Kadokawa, Polym. Bull. 64 (2010) 341;
(c) M. Setoyama, T. Kato, K. Yamamoto, J.-I. Kadokawa, J. Polym. Environ. 21 (2013) 795.

[17] J. Tang, H. Tang, W. Sun, H. Plancher, M. Radosz, Y. Shen, Chem. Commun. 26 (2005) 3325.
[18] J.G. Huddleston, A.E. Visser, W.M. Reichert, H.D. Willauer, G.A. Broker, R.D. Rogers, Green Chem. 3 (2001) 156.
[19] D.M. Fox, J.W. Gilman, A.B. Morgan, J.R. Shields, P.H. Maupin, R.E. Lyon, H.C. De Long, P.C. Trulove, Ind. Eng. Chem. Res. 47 (2008) 6327.
[20] (a) R.W. Berg, Monatsh. Chem. 138 (2007) 1045;
(b) T. Moumene, E.H. Belarbi, B. Haddad, D. Villemin, O. Abbas, B. Khelifa, S. Bresson, J. Mol. Struct. 1065–1066 (2014) 86;
(c) A.M. Moschovi, S. Ntais, V. Dracopoulos, V. Nikolakis, Vibr. Spectr. 63 (2012) 350.
[21] (a) J.D. Holbrey, W.M. Reichert, M. Nieuwnhuyzen, S. Johnston, K.R. Seddon, R.D. Rogers, Chem. Commun. (2003) 1636;
(b) O. Yamamuro, Y. Minamimoto, Y. Inamura, S. Hayashi, H. Hamaguchi, Chem. Phys. Lett. 423 (2006) 371;
(c) K. Nishikawa, S. Wang, H. Katayanagi, S. Hayashi, H. Hamaguchi, Y. Koga, K. Tozaki, J. Phys. Chem. B 111 (2007) 4894;
(d) A. Efimova, G. Hubrig, P. Schmidt, Thermochim. Acta 573 (2013) 162.
[22] C.F. Fredlake, J.M. Crosthwaite, D.G. Hert, S.N.V.K. Aki, J.F. Brennecke, J. Chem. Eng. Data 49 (2004) 954.
[23] (a) S.V. Dzyuba, R.A. Bartsch, ChemPhysChem 3 (2002) 161;
(b) H. Tokuda, K. Hayamizu, K. Ishii, M.A.B.H. Susan, M. Watanabe, J. Phys. Chem. B 109 (2005) 6103;
(c) J. Troncoso, C.A. Cerdeiriña, Y.A. Sanmamed, L. Romaní, L.P.N. Rebelo, J. Chem. Eng. Data 51 (2006) 1856.
[24] A. Serghei, M. Tress, J.R. Sangoro, F. Kremer, Phys. Rev. B 80 (2009) 184301.
[25] M. Drüschler, B. Huber, B. Roling, J. Phys. Chem. C 115 (2011) 6802.
[26] (a) J.C. Dyre, T.B. Schroder, Rev. Mod. Phys. 72 (2000) 873;
(b) B. Roling, C. Martiny, S. Brückner, Phys. Rev. B 63 (2001) 214203.
[27] J. Leys, M. Wübbenhorst, C.P. Menon, R. Rajesh, J. Thoen, C. Glorieux, P. Nockemann, B. Thijs, K. Binnemans, S. Longuemart, J. Chem. Phys. 128 (2008) 64509.
[28] J.M. Hyde, T. Tomozawa, J. Non-Cryst. Solids 109 (1989) 18.
[29] (a) H. Weingärtner, J. Mol. Liq. 192 (2014) 185;
(b) M.-M. Huang, Y. Jiang, P. Sasisanker, G.W. Driver, H. Weingärtner, J. Chem. Eng. Data 56 (2011) 1494.
[30] B. Huber, L. Rossrucker, J. Sundermeyer, B. Roling, Solid State Ionics 2477 (2013) 15.
[31] W.W. Bode, Network Analysis and Feedback Amplifier Design, Van Nostrand, Princeton, NJ, 1956.
[32] M.D. Green, D. Wang, S.T. Hemp, J.-H. Choi, K.I. Winey, J.R. Heflin, T.E. Long, Polymer 53 (2012) 3677.
[33] (a) A. Jarosik, S.R. Krajewski, A. Lewandowski, P. Radzimski, J. Mol. Liq. 123 (2006) 43;
(b) G. Chatel, J.F.B. Pereira, V. Debbeti, H. Huang, R.D. Rogers, Green Chem. 16 (2014) 2051.
[34] A. Heintz, J.K. Lehmann, E. Schmidt, A. Wandschneider, J. Sol. Chem. 38 (2009) 1079.
[35] T.S. Sorensen, V. Compañ, J. Chem. Soc. Faraday Trans. 91 (1995) 4235.
[36] T.S. Sorensen, V. Compañ, R. Diaz-Calleja, J. Chem. Soc. Faraday Trans. 92 (1996) 1947.
[37] V. Compañ, T.S. Sorensen, R. Diaz-Calleja, E.R. Riande, J. Appl. Phys. 79 (1996) 403.
[38] R.J. Klein, S. Zhang, S. Duo, B.H. Jones, R.H. Colby, J. Runt, J. Chem. Phys. 124 (2006) 144903.
[39] A. Munar, A. Andrio, R. Iserte, V. Compañ, J. Non-Cryst. Solids 357 (2011) 3064.
[40] (a) P. Bruce, Chemistry of Solid State Materials: Solid State Electrochemistry, Cambrigde University Press, 1995, p. 360;
(b) J.R. Sangoro, C. Iacob, A.L. Agapov, Y. Wang, S. Berdzinski, H. Rexhausen, V. Strehmel, C. Friedrich, A.P. Sokolove, F. Kremer, Soft Matter 10 (2014) 3536.
[41] P. Bonhôte, A.-P. Dias, N. Papageorgiou, K. Kalyanasundaram, M. Grätzel, Inorg. Chem. 35 (1996) 1168.
[42] (a) A.S. Shaplov, E.I. Lozinskaya, Y.S. Vygodskii, Polymer ionic liquids: synthesis, design and application in electrochemistry as ion conducting materials, in: A.A.J. Torriero, M.J.A. Shiddiky (Eds.), Electrochemical Properties and Applications of Ionic Liquids, Nova Science Publishers, 2010 (Chapter 10);
(b) H. Ohno, Electrochim. Acta 46 (2001) 1407;
(c) R. Marcilla, F. Alcide, H. Sardon, J.A. Pomposo, D. Mecerreyes, Electrochem. Commun. 8 (2006) 482;
(d) Y.S. Vygodskii, O.A. Mel'nik, E.I. Lozinskaya, A.S. Shaplov, I.A. Malyshkina, N.D. Gavrilova, K.A. Lyssenko, M.Y. Antipin, D.G. Golovanov, A.A. Korlyukov, N. Ignat'ev, U. Wels-Biermann, Polym. Adv. Technol. 18 (2007) 50.
[43] (a) H. Nakajima, H. Ohno, Polymer 46 (2005) 11499;
(b) K. Põhaki-Esko, M. Timusk, K. Saal, R. Lõhmus, I. Kink, U. Mäeorg, J. Mater. Res. 22 (2013) 3086.